Hindawi
Applied and Environmental Soil Science
Volume 2021, Article ID 5753942, 21 pages
https://doi.org/10.1155/2021/5753942

Research Article

Geospatial Analysis of Soil Erosion including Precipitation Scenarios in a Conservation Area of the Amazon Region in Peru

Ligia García,[1] **Jaris Veneros**,[1] **Franz Pucha-Cofrep**,[2] **Segundo Chávez**,[1] **Danilo E. Bustamante**,[3] **Martha S. Calderón**,[3] **Eli Morales**,[3] **and Manuel Oliva**[3]

[1]*Instituto de Investigación,Innovación y Desarrollo para el Sector Agrario y Agroindustrial de la Región Amazonas IIDAA, Universidad Nacional Toribio Rodríguez de Mendoza de Amazonas,Perú, Calle Higos Urco No. 342-350-356-Calle Universitaria No. 304, Amazonas, Peru*
[2]*Departamento de Geología, Minas e Ingeniería Civil (DGMIC), Hidrología y Climatología Working Group, Universidad Técnica Particular de Loja, Ecuador, Calle París No. 1101608, de Loja, Ecuador*
[3]*Instituto de Investigación para el Desarrollo Sustentable de Ceja de Selva INDES-CES, Universidad Nacional Toribio Rodríguez de Mendoza de Amazonas,Perú, Calle Higos Urco No. 342-350-356-Calle Universitaria No. 304, Amazonas, Peru*

Correspondence should be addressed to Jaris Veneros; jaris.veneros@untrm.edu.pe

Received 19 May 2021; Accepted 13 August 2021; Published 8 September 2021

Academic Editor: Fedor Lisetskii

The Tilacancha Private Conservation Area provides fresh water to the city of Chachapoyas. Therefore, the amount of soil lost in the year and under precipitation scenarios was determined. Individually, the values of the factors were obtained: rain erosivity (R) in 2019 and simulating increase and decrease of 15% of rainfall, soil erodibility (K), length and degree of slope (LS), land cover (C), and conservation practices (P); they were integrated into USLE, obtaining $A = R * K * \text{LS} * \text{PC}$, (t/ha.yr). Six ranges of erosion were found, and the ACP had areas where from 0.4 to 665.20 t/ha.yr of soil was lost. A 15% reduction in rainfall would represent a loss of soil from 0.20 to 301.56 t/ha.yr and an increase in rainfall by 15%, and the erosion ranges would vary from 0.2 to 1028.84 t/ha.yr.

1. Introduction

Peru has two types of nongovernmental protected areas: Private Conservation Areas (ACPs) and conservation concessions [1]. Tilacancha is one of the 141 ACPs [2], created by Resolution of the Ministry of Environment, on July 6, 2010, for 20 years, and is located in Chachapoyas, Amazon region in northern Peru [3]. According to the Ecosystem Map of Peru, the Tilacancha ACP has 6800.48 ha and it presents four ecosystems: Yunga Altimontane Forest (pluvial), Jalca, Pastures/Herbazales, and secondary vegetation [4].

The Tilacancha ACP is the only source of water for the city of Chachapoyas, and this city has a population of more than 32 thousand inhabitants [5]. The current overexploitation of water resources in Peru [6], the growing demand of households for freshwater [7], and the increase in world consumption increased almost eight times during the last century [8].

Currently, the ACP is threatened by anthropic factors such as agriculture, livestock, deforestation, slashing, and burning of grasslands and natural forests, which degrade the soil [3, 5]. Also, despite the known benefits of plant communities when they grow, they modify the physical, chemical, biological, and other properties of the soil, with consequent effects on plant survival and growth [9], and the loss of soil is progressive and is considered an irreversible phenomenon [10].

Soil erosion affects the storage, filtering, and cleaning of water, as well as the habitats and genetic reserves of species [11, 12]. Water erosion in the world is intensified because different climatic conditions and land use to act on the various natural conditions, mold the soil, and, on certain

occasions, degrade it [13]. This implies that providing a perspective view of the effects of climate change on soil loss can guide decision makers in environmental management and planning [14].

Agroecosystems and buffer zones around the ACP depend on ecosystem conditions and regulating ecosystem services, for example, the action of vegetation cover against soil erosion or as a function of water quality and quantity. Likewise, the replacement of forest by other land uses can cause serious impacts on the quality of river water, altering its physical, chemical, and biological characteristics, so Permanent Preservation Areas (PPAs) should be established, in order to assess the variability of its quality because it has been shown that degraded watersheds presented higher values of solids, turbidity, nutrients, and coliforms, in addition to presenting greater variability of temporal data compared to forested watersheds [15]. Thus, assessments of ecosystem services, conditions, and interactions are very important to understand the relationships in highly managed systems [16].

The results obtained in this research, on estimating the spatial distribution of current water erosion and under scenarios of ±15% of rainfall for the Tilacancha ACP, provide an urgent response to the need to map, not only the current state of the water erosion index but also to determine the influences of climate change scenarios [17], and the results will be used to manage and avoid the water erosion of the soil in the ACP for its conservation.

2. Materials and Methods

2.1. Study Area. The Tilacancha ACP is located between 2700 and 3490 m.a.s.l. in the stream of the same name, within the Utcubamba River basin, a tributary of the Marañón River, in the Amazon region of Peru (Figure 1). This ACP is located on lands of the communities of San Isidro de Maino and Levanto and has an area of 6,800.48 ha [18].

2.2. Implementation of Available Datasets into USLE. To determine the loss of soil due to water erosion in the ACP, the USLE equation was used [19], where five factors are used that are finally integrated into equation (1). The methodological process is shown in Figure 2.

The function that describes the estimation of water erosion is expressed as follows [20–23]:

$$A = R * K * \mathrm{LS} * C * P, \tag{1}$$

where A: average annual soil loss expressed in T/ha.yr, R: rain erosivity factor expressed in kinetic energy per unit area in MJ $*$ mm $*$ ha^{-1} $*$ h^{-1} $*$ year^{-1}, K: soil erodibility factor expressed in T $*$ ha $*$ h $*$ MJ^{-1} $*$ mm^{-1} $*$ ha^{-1}, LS: length factor and grade of slope, C: plant cover factor, and P: applied conservation practices factor.

The R factor represents the erosivity factor of the rain, and it refers to the sum of all the annual rain events and their respective maximum intensities, which gives us an idea of the degree of aggressiveness of precipitation to soil degradation. Wischmeier and Smith [19] represented an erosivity index based on the direct relationship between kinetic energy (E) and the intensity of rain (I) [24] (Figure 3(a)). Equation (2) [10] measured in MJ $*$ mm $*$ ha^{-1} $*$ h^{-1} $*$ year^{-1} was used:

$$R = I_{30} * \frac{9.28P - 8.393}{1000}, \tag{2}$$

where I_{30}: 75 mm/h, the value recommended by Wischmeier [25], and P: annual mean precipitation (mm). The precipitation values for the Tilacancha ACP were obtained from the Global Climate Data, Worldclim version 2, which contain meteorological data worldwide from the 1970s to the 2000s with a resolution 1 km^2 [26, 27]. The data were extracted using the "extract by mask" tool of the ArcGis 10.7 program; this tool allows you to extract a part of a raster dataset based on a template extension. The clip output includes the pixels that intersect with feature datasets for the ACP. Besides, this methodology solved the lack of information on precipitation data in the place, as happens in several regions of the world [28, 29]. The evaluation ranges were considered in five scales and are the following [30]: 144–213 MJ $*$ mm $*$ ha^{-1} $*$ h^{-1} $*$ year^{-1}; 214–248 MJ $*$ mm $*$ ha^{-1} $*$ h^{-1} $*$ year^{-1}; 249–285 MJ $*$ mm $*$ ha^{-1} $*$ h^{-1} $*$ year^{-1}; 286–319 MJ $*$ mm $*$ ha^{-1} $*$ h^{-1} $*$ year^{-1}; and 320–355 MJ $*$ mm $*$ ha^{-1} $*$ h^{-1} $*$ year^{-1} (Figure 3(a)).

The erodibility index (K factor) measures the susceptibility of the soil to water erosion [11], and the K factor in the International System of Units is expressed in T $*$ ha $*$ h/MJ.mm $*$ ha, which expresses the resistance of the soil in surface and time, concerning the energy of rain [31]. It was obtained directly through the following equation (Figure 3(b)):

$$\mathrm{K} = 1.313 * \frac{\left[2.1 * 10^{-4} * (12 - \mathrm{MO}) * \mathrm{M}^{1.14} + 3.25 * (\mathrm{s} - 2) + 2.5 * (\mathrm{p} - 3)\right]}{100}, \tag{3}$$

where OM: percentage of organic matter (OM) of the samples, s: soil structure code, p: permeability code, and M: factor given by the product of the sum of the percentages of silt and very fine sand with the sum of the percentages of sand and silt. That is, (%silt + very fine sand) $*$ (100 − %clay).

The textural class was obtained by the Bouyoucos Method [32], from a total of 108 soil samples representative of the ACP [33, 34] resulting in five classes: sandy (S), sandy loam (SL), loam (S), loamy sand (LS), and sandy clay loam (SCL) (Figure 4(a)). Organic Matter was obtained with the

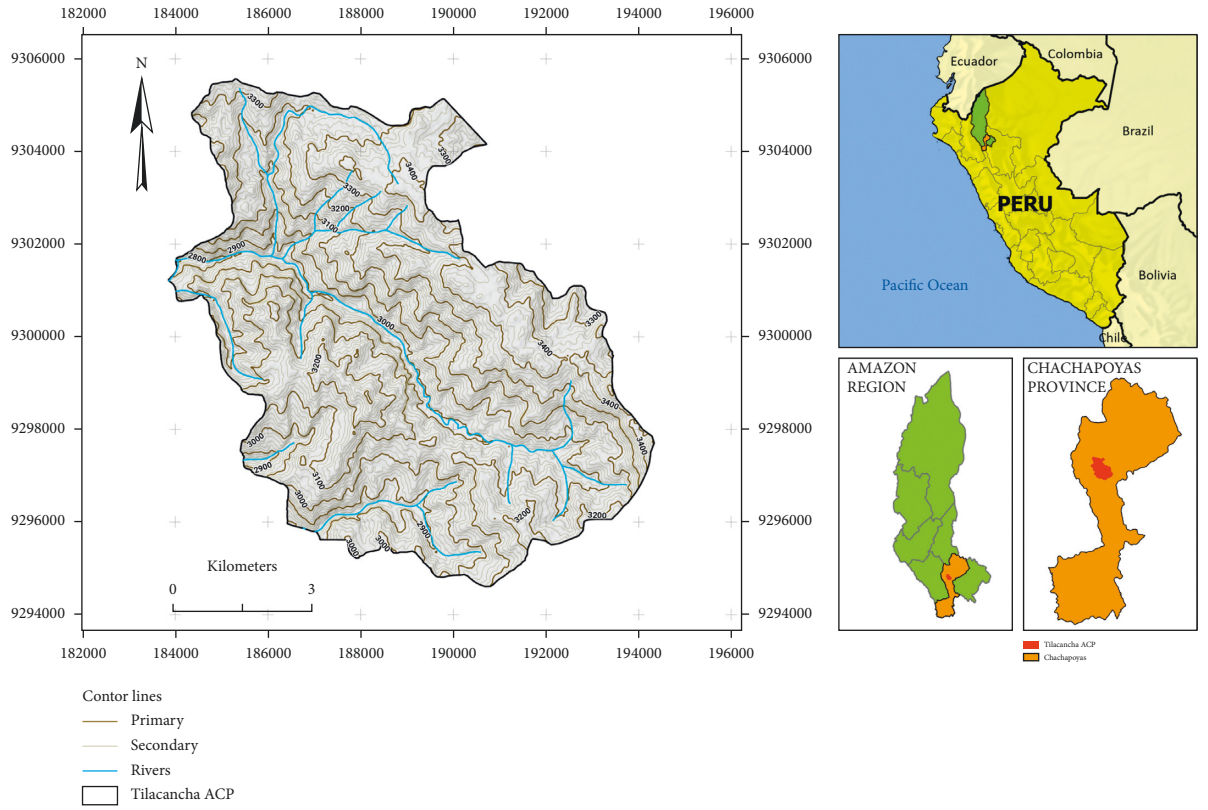

Figure 1: Location of the Tilacancha ACP.

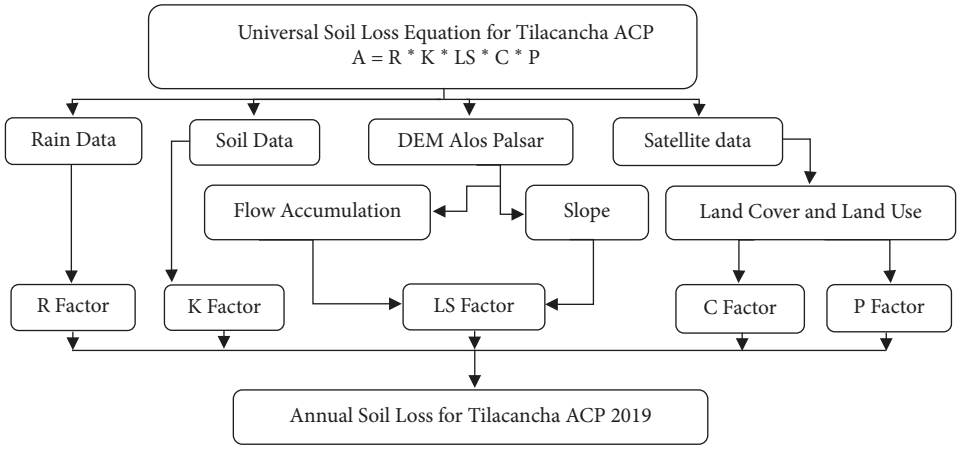

Figure 2: Methodological flow to integrate the Universal Soil Loss Equation (USLE), adapted from the work of Rizeei et al. [13], where *A* is annual soil loss in the Tilacancha ACP for 2019, *R* factor: rain data, *K* factor: soil data, LS factor: flow and slope accumulation, *C* factor: land cover and land use, and P factor: conservation practices.

Walkley and Black method [35], with ranges from 1.9 to 9.9% (Figure 4(b)).

The LS factor (Figure 3(c)) was calculated using the interaction between the topography, percentage, and length of the slope and the accumulation of flow [36, 37]. The flow direction and flow accumulation model were implemented with the ArcHydro extension for ArcGIS [38, 39]. The Digital Elevation Model (DEM) was obtained from the Alaska Satellite Facility geoserver of the Alos Palsar Satellite with a spatial resolution of 12.5 m × 12.5 m [40–42], which allowed calculating the topographic factor (LS). The cloudless image was downloaded from the Earth Explorer portal (https://earthexplorer.usgs.gov/) of the United States Geological Survey (USGS). Landsat 8 satellite images with a spatial resolution of 30m × 30m for August 2019 were used. The slope map was implemented, and it was reclassified, obtaining the spatial distribution of the LS factor using equations (4) and (5) [39].

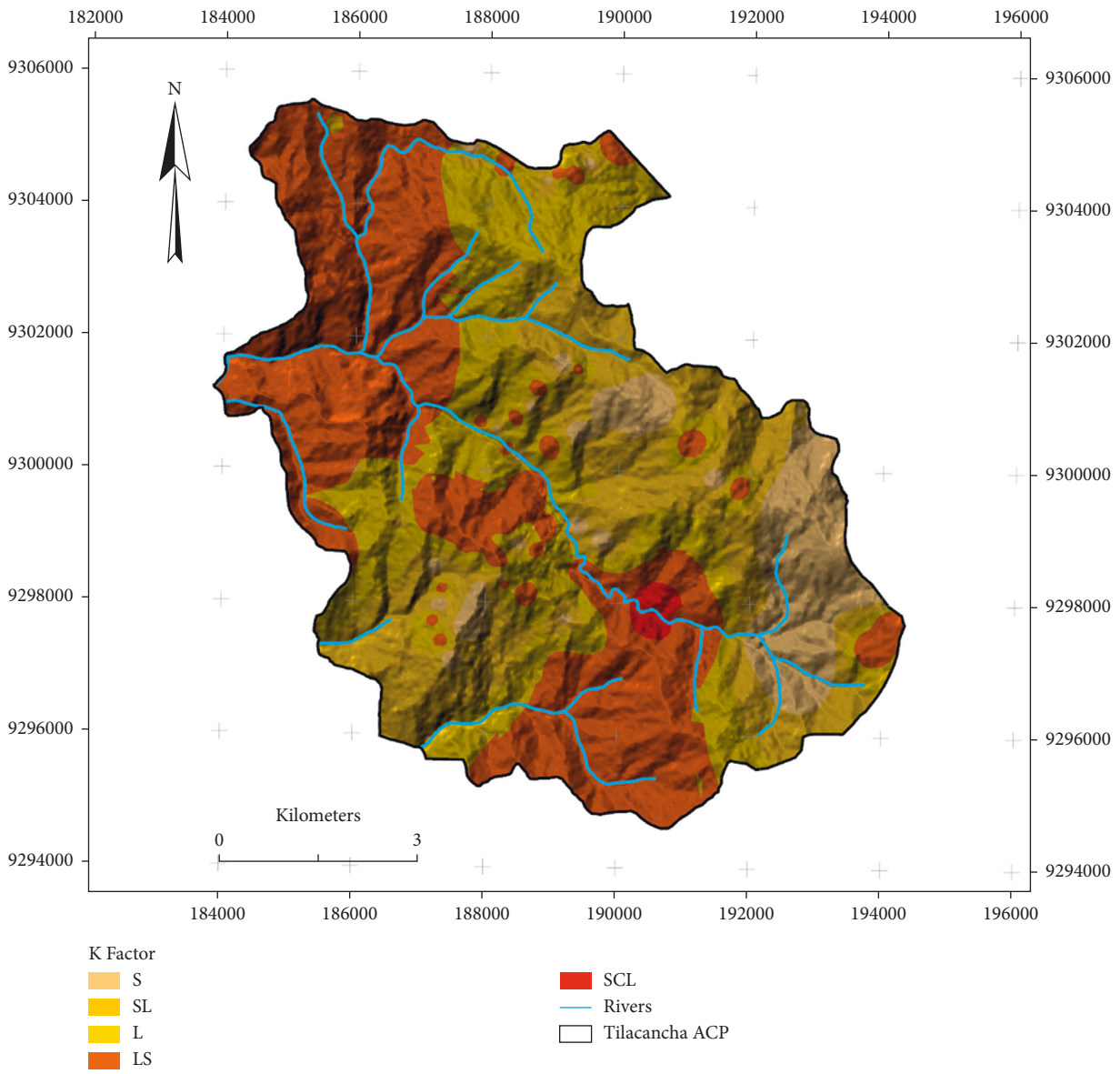

(a)

Figure 3: Continued.

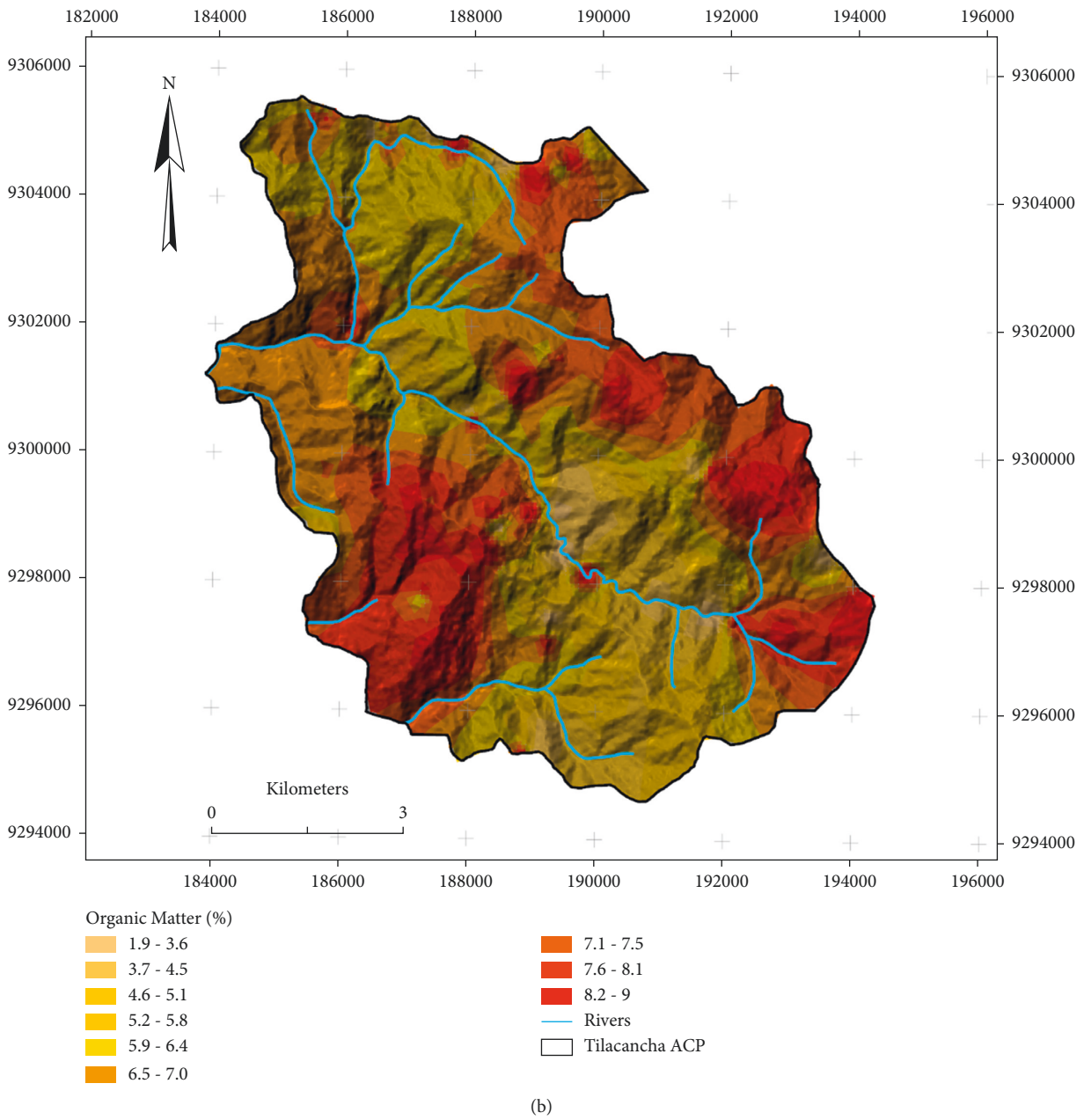

(b)

Figure 3: Maps resulting from the individual factors for the USLE calculations in the Tilacancha ACP. (a) Erosivity, (b) erodibility, and (c) LS factor.

$$\beta = \frac{(\sin(\theta/0.0896))}{3.0(\sin\theta)^{0.8} + 0.56}, \quad (4)$$

where θ = the angle of the slope according to Flores-López et al. [43]. In ArcMap with Raster Calculator, the following formula is used to obtain the factor β, where factor β = ((sin ("Slope" * 0.01745)/0.0896)/
(3 * Power(Sin("Slope" * 0.01745), 0.8)) + 0.56)). Once the factor β was obtained, the M factor was obtained. Equation (7) is used in the "Raster Calculator."

$$m = \frac{\beta}{(\beta + 1)}, \quad (5)$$

where M factor = "Factor_β"/("Factor_β" + 1).

The calculation of the L factor with the contributing drainage area was carried out with the Flow Direction and Flow Accumulation tools, respectively. Once these two images were obtained, the L factor (equation (6) using equation (5)) was obtained [44, 45].

$$L_{(i,j)} = \frac{\left(A_{(i,j)} + D^2\right)^{m+1} - A_{(i,j)}\, m + 1}{x^m + D^{m+2} * (22.13)^m}, \quad (6)$$

where $A(i, j)$ [m] = the unit contributing area at the input of a pixel, D = the size of the pixel, and X = the shape correction factor. L factor = (Power(("flow_acc" + 625),

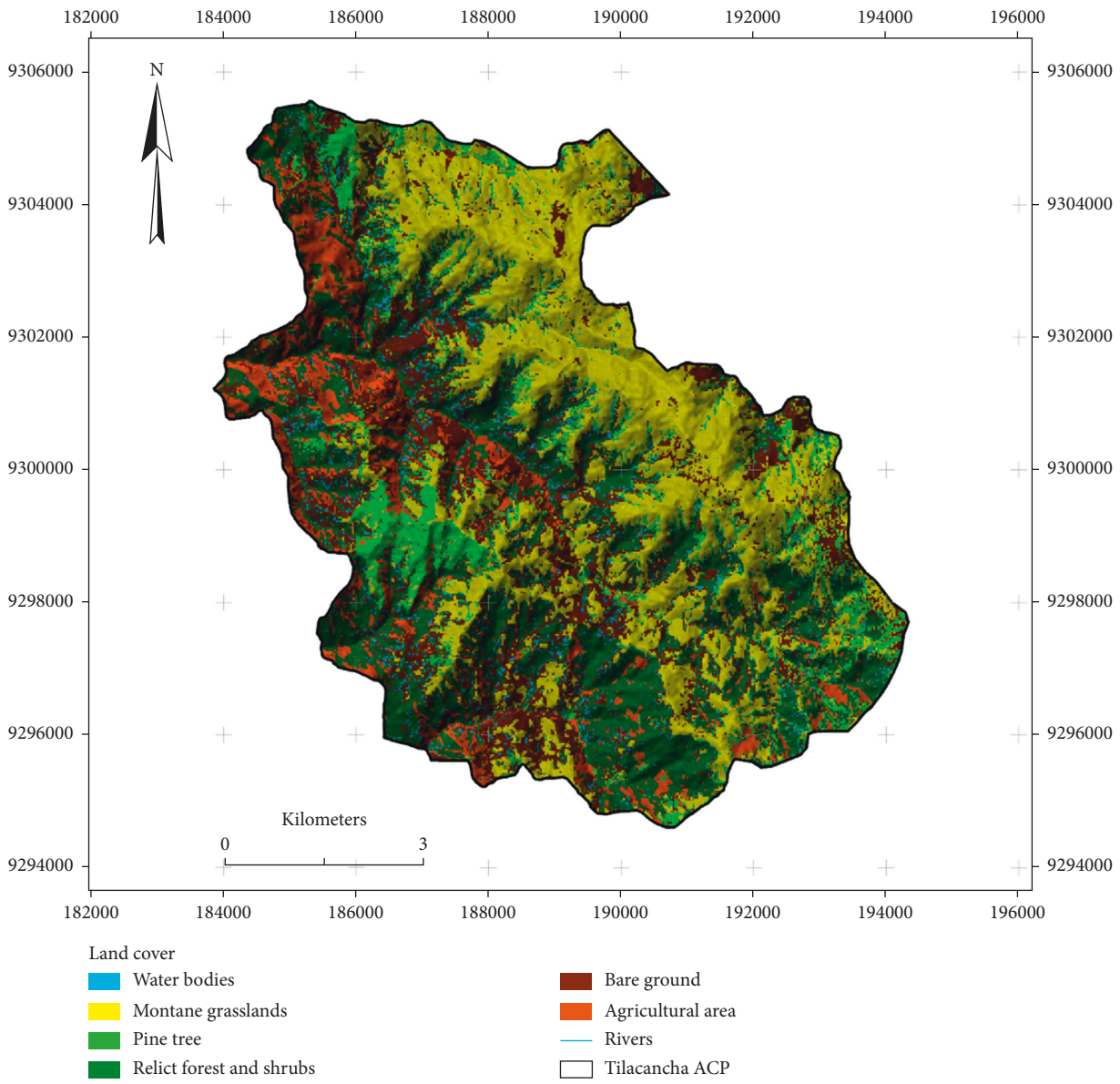

Figure 4: Resulting maps to determine the K factor: (a) soil texture and (b) organic matter in the Tilacancha ACP.

("Factor_M" + 1))Power ("flow_acc," ("Factor_M" + 1))))/ Power(25, ("Factor_M"+2)) ∗ Power(22, 13"Factor_M")), which refers to equation (6).

Otherwise, to calculate factor S, the following equation was used:

$$S_{(i,j)} = \begin{cases} 10.8 \sin \beta_{(i,j)} + 0.03, & \tan \beta_{(i,j)} < 0.09, \\ 16.8 \sin \beta_{(i,j)} - 0.5, & \tan \beta_{(i,j)} \geq 0.09, \end{cases} \quad (7)$$

where $S(i, j)$ = slope of the coordinate factor (i, j)·and $\beta(i, j)$ = slope in degrees with coordinates (i, j). S factor = with ((tan ("Slope" * 0.01745) <0.09), (10.08 * sin ("Slope" * 0.01745) + 0.03), (16.8 * Sin ("Slope" * 0.01745)) − 0.5)), which refers to equation (8). The subfactor raster of (S) is the slope of the terrain, where the angle is taken as the mean angle to all subgrids in the direction of the steepest slope [38]. When this formula is applied in the ArcGIS Raster Calculator, it must be considered that the angle has to be converted to radians [39]. Once all the previous factors had been obtained, the LS factor that is the object of this methodology was calculated. For this, equation (8) was used, which refers to equations (6) and (7) (Figure 3(c)). This figure has the following ranges for the slope in percent (%): o: 0–3; p: 4–12; q: 13–18; r: 19–24; s: 25–30; t: 31–60, u: 61–70, v: 71–100, and w: >101.

$$\text{LS Factor} = \text{"Factor\_L"} * \text{"Factor\_S."} \quad (8)$$

The C factor ranges from 0 to 1 (Table 1). A value equal to 1 indicates that there is no cover and the surface is treated as barren soil, while a C value close to 0 indicates very strong cover effects and well-protected soil [19, 23]. For the calculation of C factor, the supervised classification technique [46] was used, through Landsat 8. The types of land cover within the Tilacancha ACP were determined with the supervised classification technique [46], using Landsat 8 Image

Table 1: Soil coverage (*C* factor) for ACP Tilacancha.

Cover type	Color	Area (ha)	Percentage	*C* factor
Water bodies		104.34	1.53	—
Montane grasslands		2246.82	33.04	0.10
Pine tree		766.79	11.28	0.01
Relict forests and shrubs		1760.42	25.89	0.01
Bare ground		1367.3	20.11	1.00
Agricultural areas		554.81	8.16	0.70
Total		6800.48	100	—

from August 18, 2019. The atmospheric correction of their bands was performed through QGIS 3.14 software [47], and to obtain an image of natural color, a combination of bands (4-3-2) was performed using the ArcGis software [48].

The classification of land cover has six types of predominant classes [49, 50] (Table 1 and Figure 5): water bodies, montane grasslands, pine tree, relict forests and shrubs, bare ground, and agricultural areas. Likewise, the numerical value of the C factor was determined from the literature review due to the lack of this information for local conditions [51–53] and was entered into the USLE equation.

The bodies of water correspond to lakes, lagoons, rivers, and springs. Otherwise, the paramo is the neotropical alpine wetland ecosystem that is covering the highest region of the Northern Andes [54]. The grasslands predominate the area and are located in the upper middle part of the mountains that delimit the ACP. Pine forests are distributed in high areas and with not very steep slopes in the ACP. Similarly, the relict and shrub forests correspond to areas of trees and natural shrubs that remained as a vestige of what once existed. The areas of bare soil are distributed mainly in the middle and upper parts of the ACP and with not very steep slopes; these zones are made up of areas without coverage and highly exposed to erosion. The agricultural area is made up of coverage with crops and pastures and is located mostly in the lower and middle parts of the ACP.

The conservation practices factor (P) has values between 0 and 1 [55]. To calculate the PC values, we use the methodology proposed by Gelagay and Minale [56]. Factor P does not present units of measurement, and the value of 1.0 [50] was used since, in the Tilacancha ACP, conservation practices are not applied. Finally, Figure 6(b) corresponds to the potential erosion t/ha.yr considering the *R* factor, K factor, LS factor, and P factor.

2.3. Simulation under Two Scenarios of Soil Loss Due to Water Erosion for the R Factor (Erosivity) Values. In Figure 7, the methodology of the two precipitation change scenarios is presented, referring to the 15% decrease and 15% increase in the coefficient of variation of precipitation (factor R) (Figure 8) in the PCA for estimating soil loss. Then, the values were integrated into the value of the erosivity factor *R* with the methodology proposed by Morgan [10] adapting the estimated values according to the following equation:

$$R = I_{30} * \frac{9.28\,(P \pm 15\%) - 8.393}{1000}, \tag{9}$$

where I30 is equal to 75 mm/h, the value which was recommended by Wischmeier [57], and P corresponds to the mean annual precipitation (mm) in ±15%. The resulting erosivity factors *R* were added to the multiplication of factors in the USLE equation. To perform the sensitivity analysis of soil loss due to water erosion in the ACP, two precipitation change scenarios were used, referring to the decrease (Figure 8(b)) and increase (Figure 8(c)) of the coefficient of variation of the historical data group for precipitation in this area (Figure 8(a)). Annual erosivity provides information on the total rainfall energy but does not provide information on the time distribution of the events [58]. The values obtained for each factor of the USLE equation were obtained in the raster format. Then, the Algebra Maps tool of the ArcGis program was applied to obtain the current erosion map and the two water erosion susceptibility maps under two scenarios.

3. Results

The estimate of the amount of soil lost in the Tilacancha ACP, for the year 2019, has values from 0.4 to 665.2 t/ha.yr, represented in the distribution spatial analysis of the ACP, cataloging the soil loss in six ranges that go from low to extreme (Table 2 and Figure 6).

The low range of erosion (light green color in Figure 6 and Table 2) had soil losses from 0.4 to 50 t/ha.yr, that is, 31.1% of the total area of the ACP. When estimating the erosion decrease and increase in 15%, the level of erosion was determined by 56.48% and 5.8%, respectively. Similarly, the average range of erosion is represented by the dark green color in Figure 6 and Table 2, with soil losses from 51 to 100 t/ha.yr, and this corresponds to 2251 ha, that is, 33.1% of the total area of the ACP.

When estimating erosion with a 15% decrease in annual precipitation, a decrease of the level of erosion was determined by 20.29% and an increase of 2.1%. Soil erosion ranging from 101 to 150 t/ha.yr corresponds to the considerable range, represented by the yellow color in Figure 6 and Table 2, where there is 1414 ha with this erosion range and corresponds to 20.8% of the total area of the ACP in 2019. An increase and decrease of 15% in precipitation led to an increase in area with

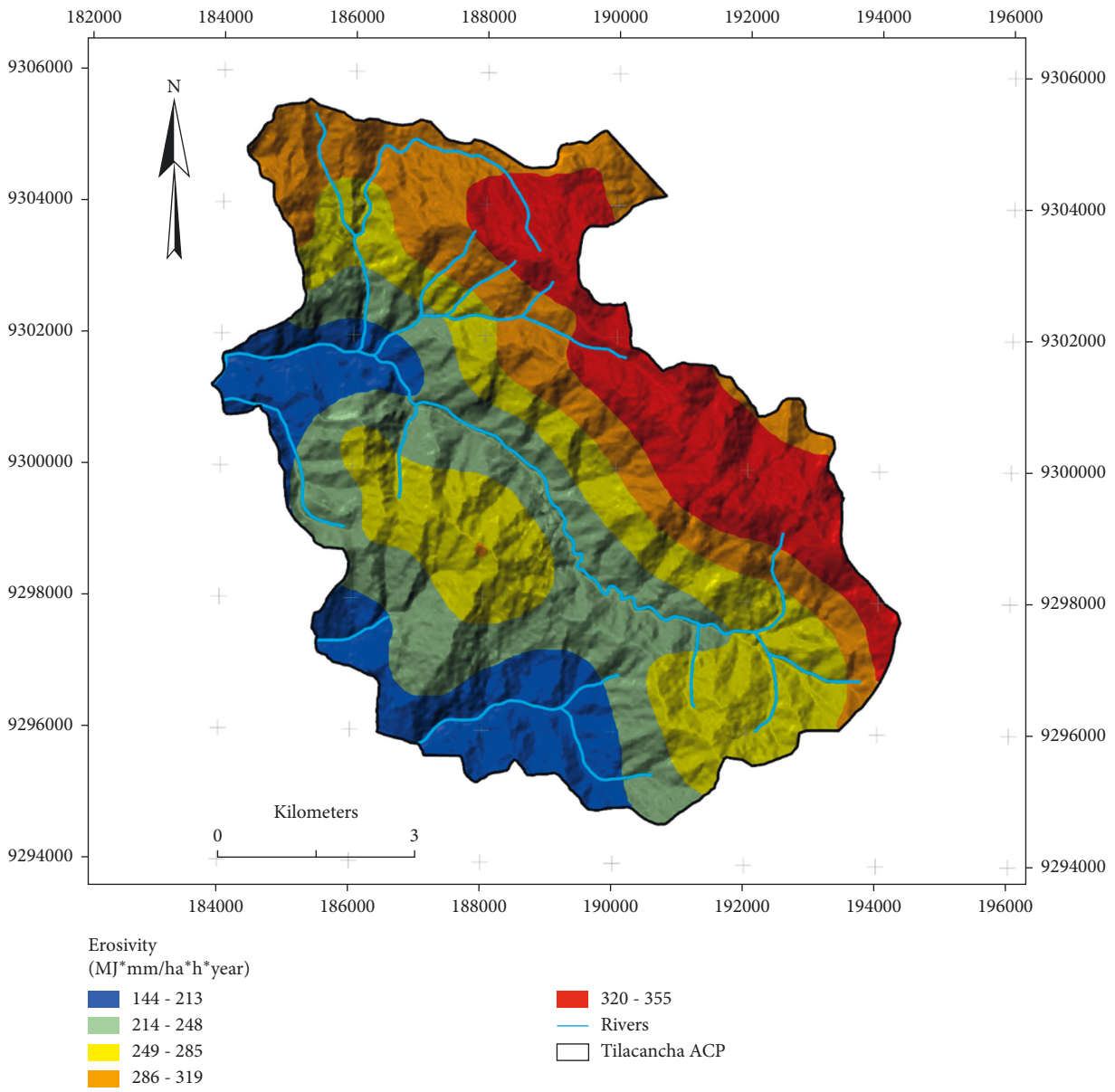

(a)

Figure 5: Continued.

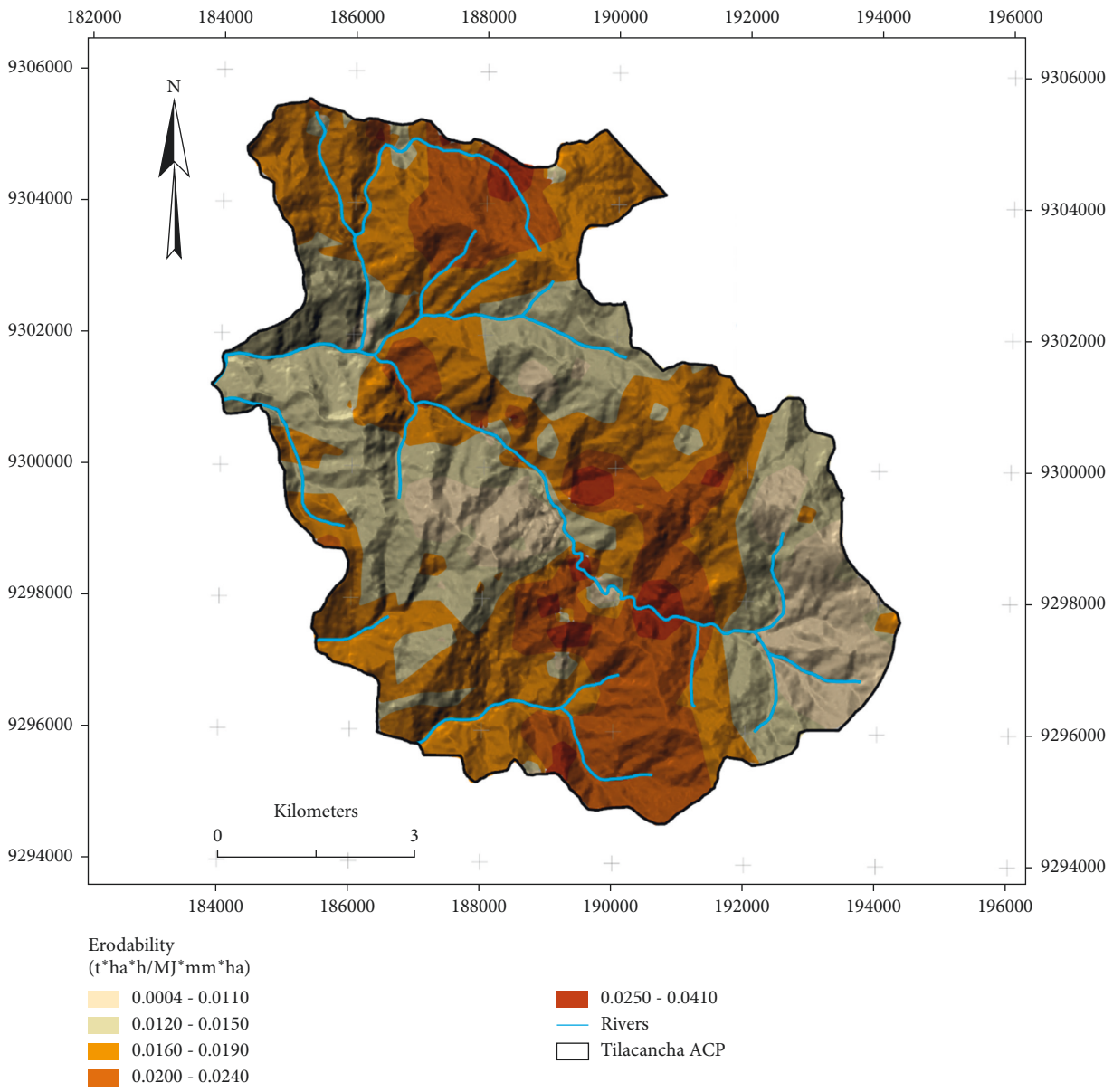

(b)

Figure 5: Continued.

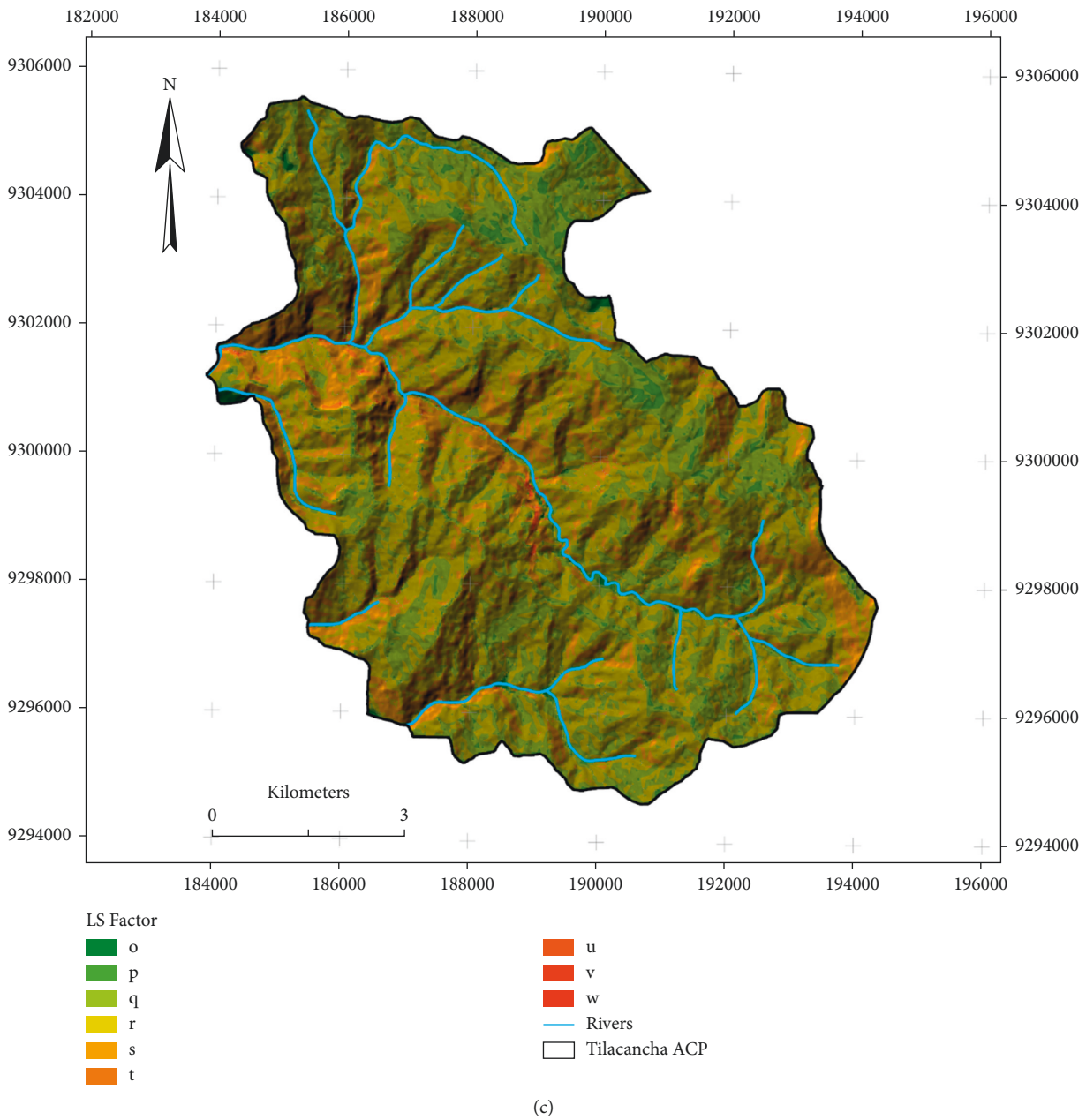

(c)

Figure 5: Land cover map for the Tilacancha ACP (*C* factor).

considerable erosion ranges of +2.1% and a reduction of −20.29% in these areas. The loss of soil erosion of high range, brown color in Figure 6 and Table 2, ranges from 151 to 200 t/ha.yr and represents 11.3% of the total area of the ACP, and the estimates with an increase and a decrease of the 15% of precipitation show a decrease in soil loss in the number of areas of 11.26% and 0.6%, respectively.

Following, there is 238.33 ha that corresponds to 3.5% of the area of the ACP and corresponds to the ranges of soil loss from 201 to 250 t/ha.yr, pink in Figure 6 and Table 2, and these represent very high ranges of erosion. The estimates of −15% and +15% of precipitation estimated a change of areas for this level of erosion with a decrease of 3.49% and an increase of 0.32%, respectively. Finally, the red color in the maps in Figure 6 represents extreme soil erosion, that is, values of soil loss that are equal to or greater than 251 t/ha.yr. In the ACP, it represents a value of 0.26% of the area for the year of study; the estimates of soil loss with an increase and decrease of 15% in precipitation result in variations of −0.259% for the current range when it occurs a decrease in precipitation; on the contrary, a 15% increase in precipitation shows an increase in areas for the ACP by 1.78%.

For the entire ACP, the following values of soil loss due to water erosion were presented: in 2019, a minimum value of 0.4 t/ha.yr and a maximum value of 665.2 t/ha.yr and total average 60 t/ha.yr with a standard deviation of 38.8%. With a scenario of a 15% reduction in average annual precipitation, a minimum erosion value of 0.20 t/ha.yr is estimated, a

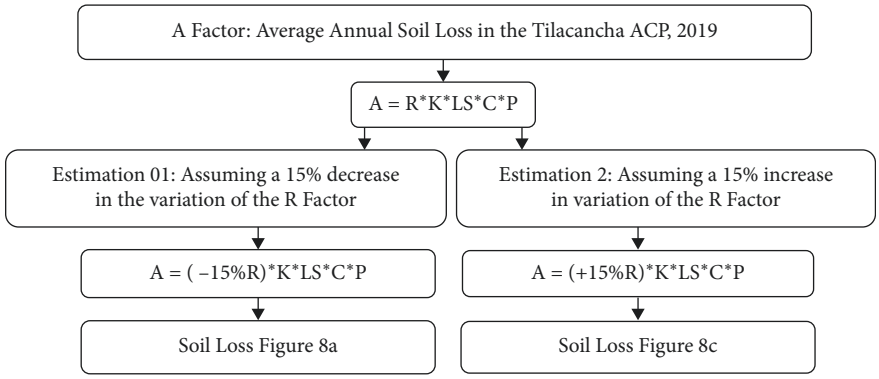

Figure 6: Estimation of water erosion using USLE in the Tilacancha ACP: (a) estimated water erosion with −15% of annual pp, (b) current water erosion with annual pp, and (c) estimated water erosion with an increase of +15% of annual pp.

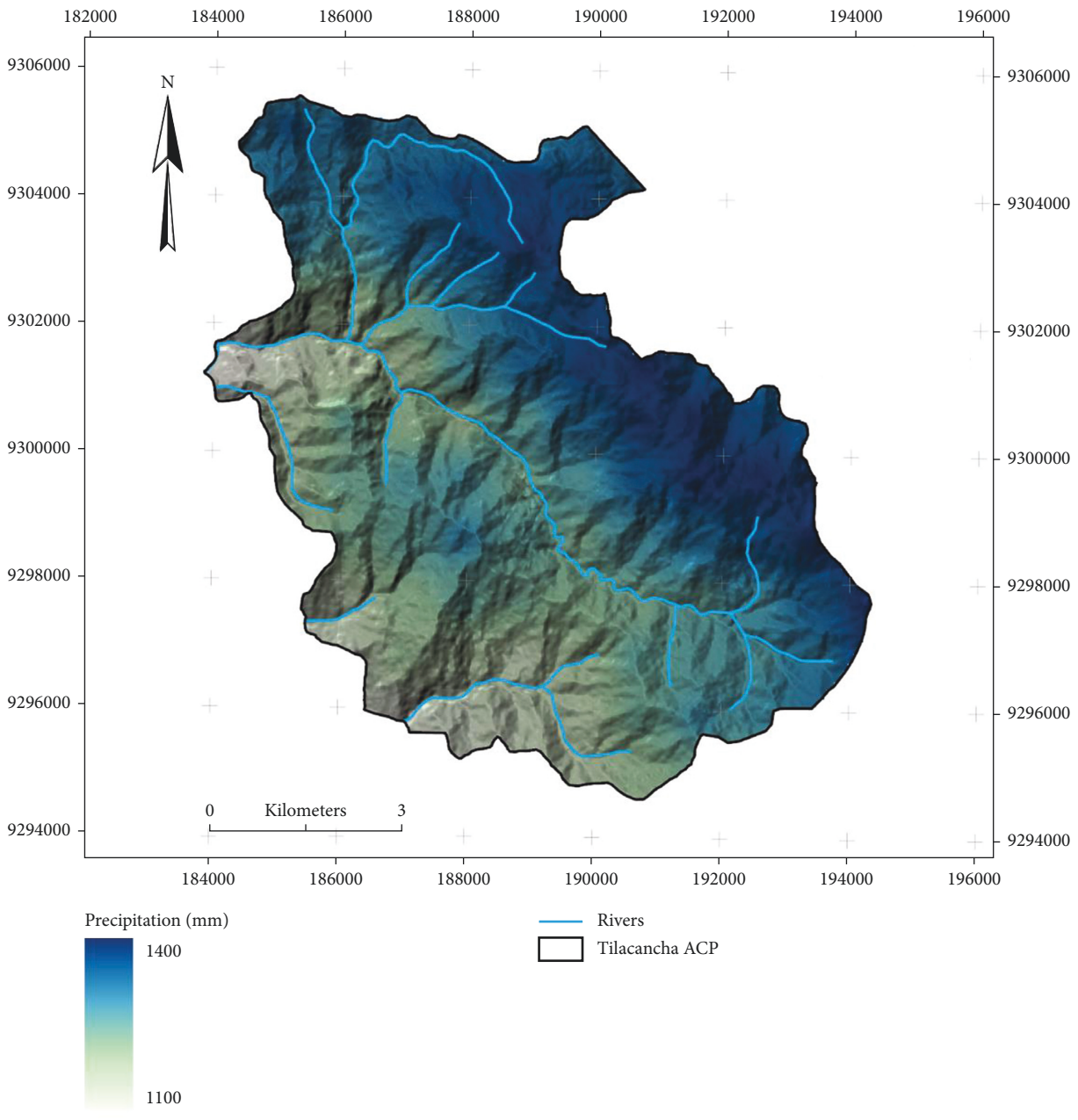

(a)

Figure 7: Continued.

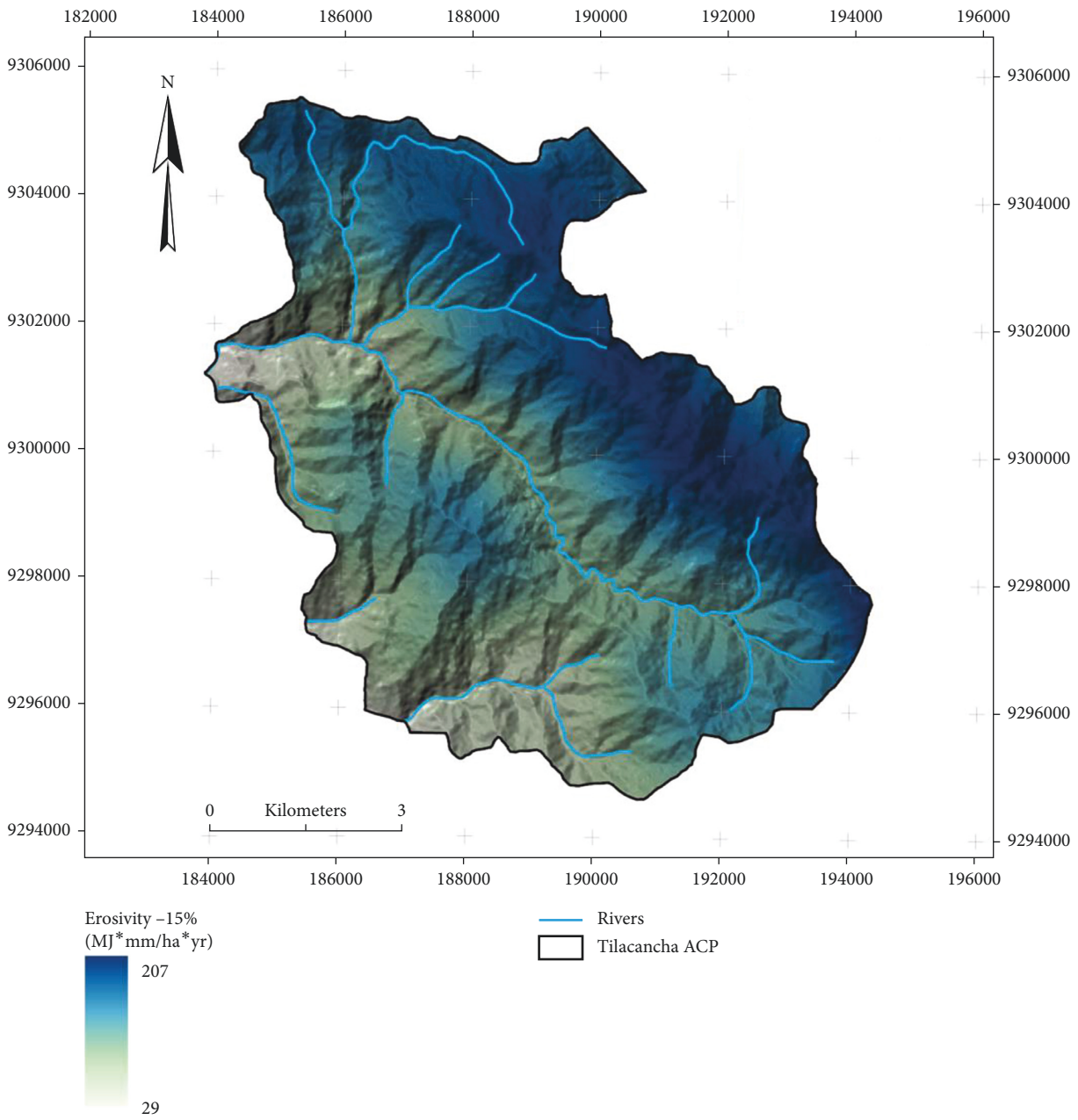

(b)

Figure 7: Continued.

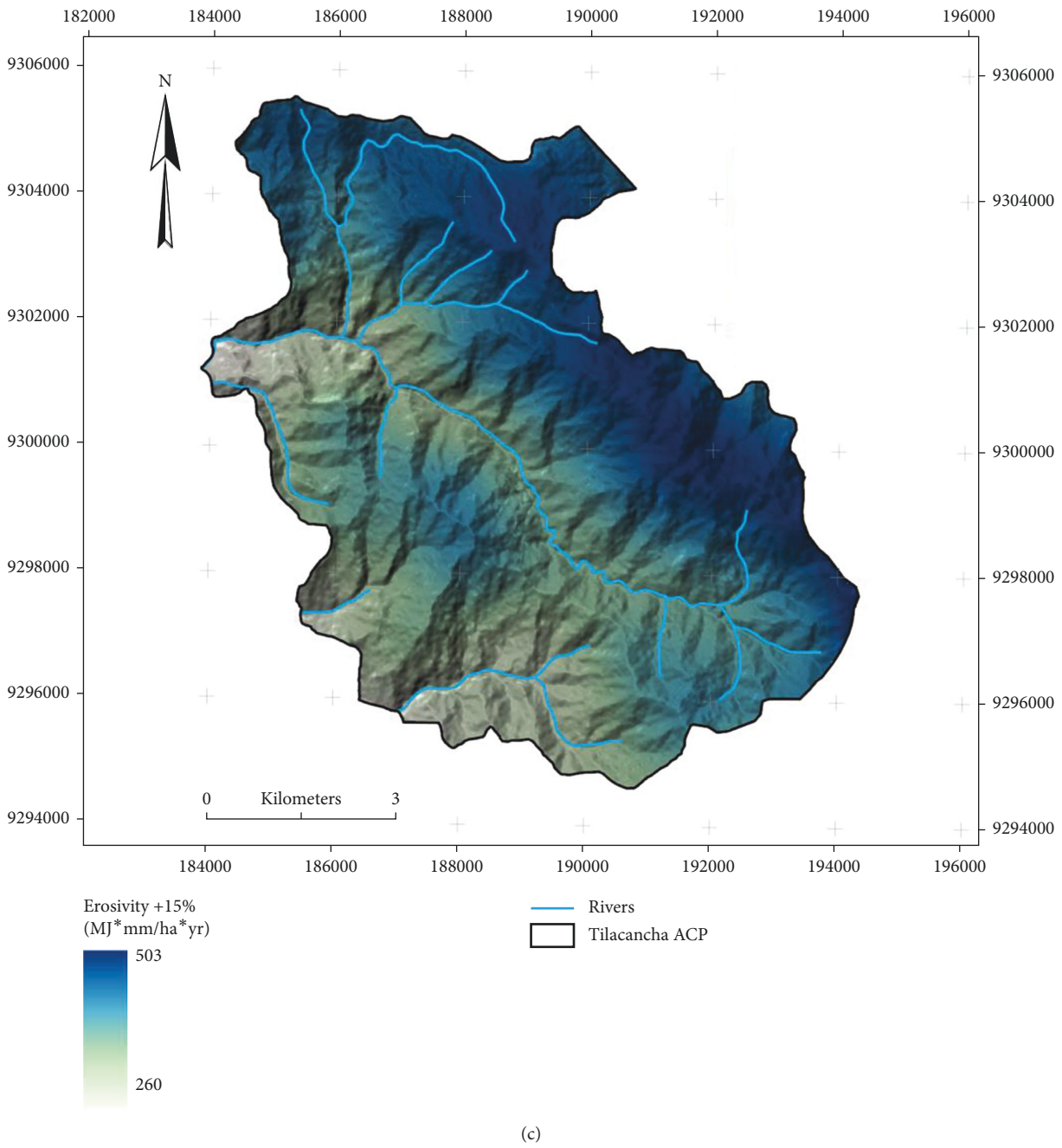

(c)

Figure 7: Methodological flow for the simulation under two scenarios of soil loss due to water erosion for values of the *R* factor (erosivity), in the Tilacancha ACP, where factor *A* is the average annual soil loss in the Tilacancha ACP in 2019.

maximum value of 301.56 t/ha.yr and an average value of 28.50 t/ha.yr with a standard deviation of 18.49%. Otherwise, the erosion estimate when increasing 15% of annual precipitation resulted in a minimum value of 0.2 t/ha.yr, which can reach maximum values of 1028.84 t/ha.yr, and an average total of 61.59 t/ha.yr with a standard deviation of 60.0%.

4. Discussion

The soil erosion estimates from our study were possible using USLE [59], thanks to the wide use of the model to efficiently predict soil erosion under different conditions [19, 25]. USLE generated information that allows determining specific strategies according to the volume and the spatial distribution of soil erosion, as Gaspari et al. [13] did, defining and selecting cultivation and management combinations for adequate control of erosion in a Serrana Bonaerense Basin, Argentina. The precision and accuracy of DEMs become increasingly important as we expand their use for the spatial prediction of soil attributes [60].

The work of Basuki et al. [61] agrees with this research, since using the DEM called ALOS PALSAR with a resolution

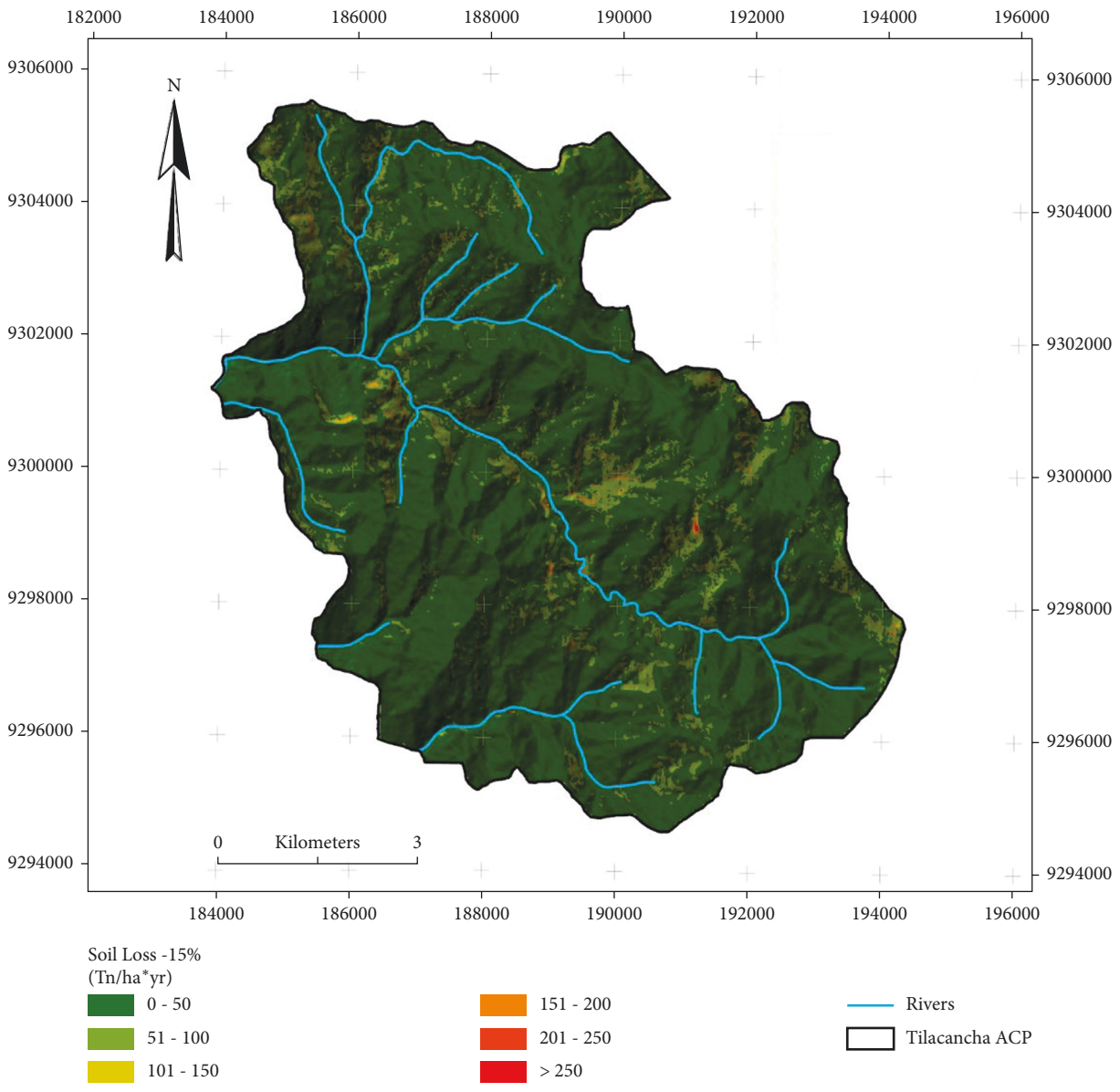

(a)

Figure 8: Continued.

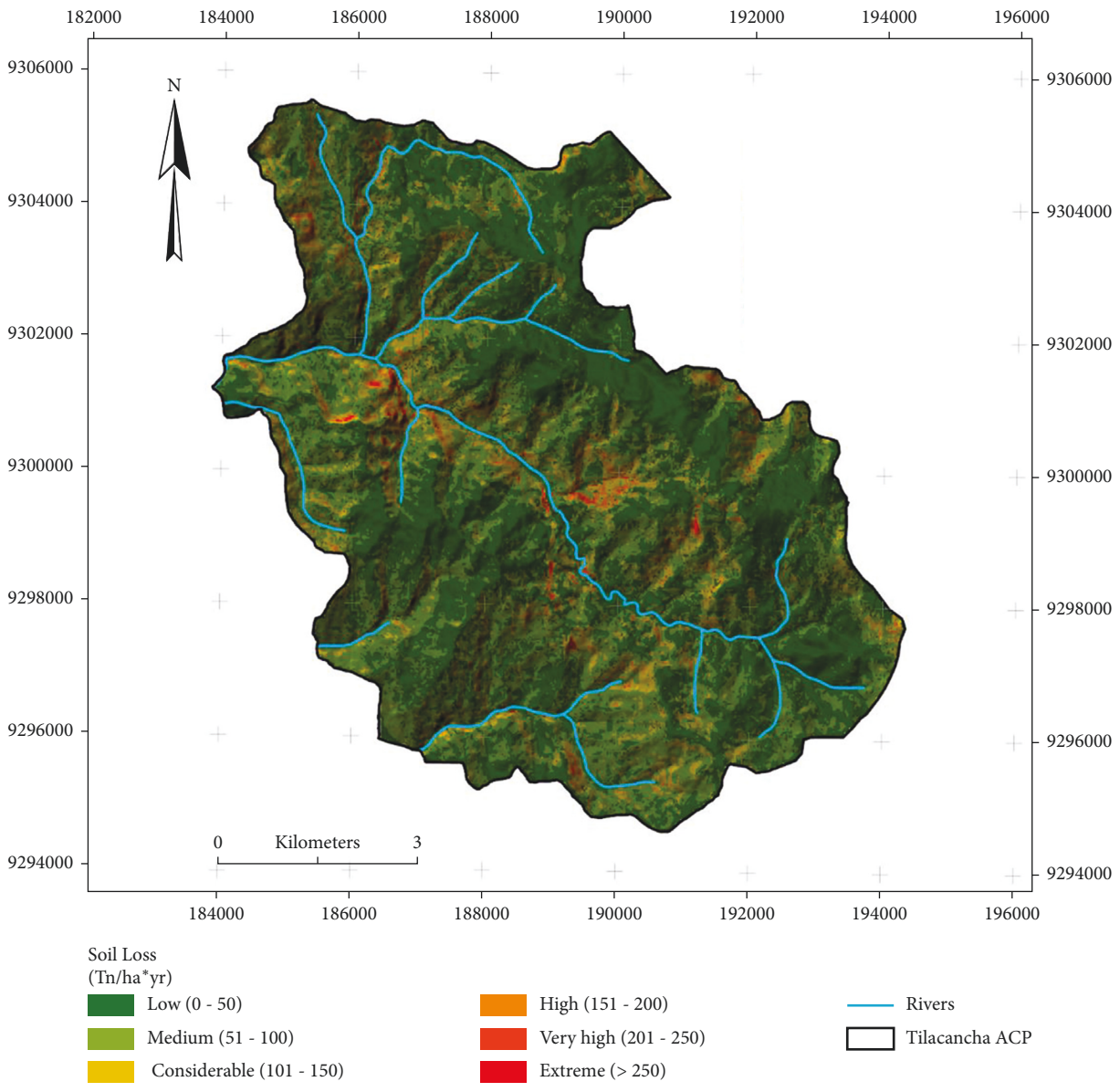

(b)

Figure 8: Continued.

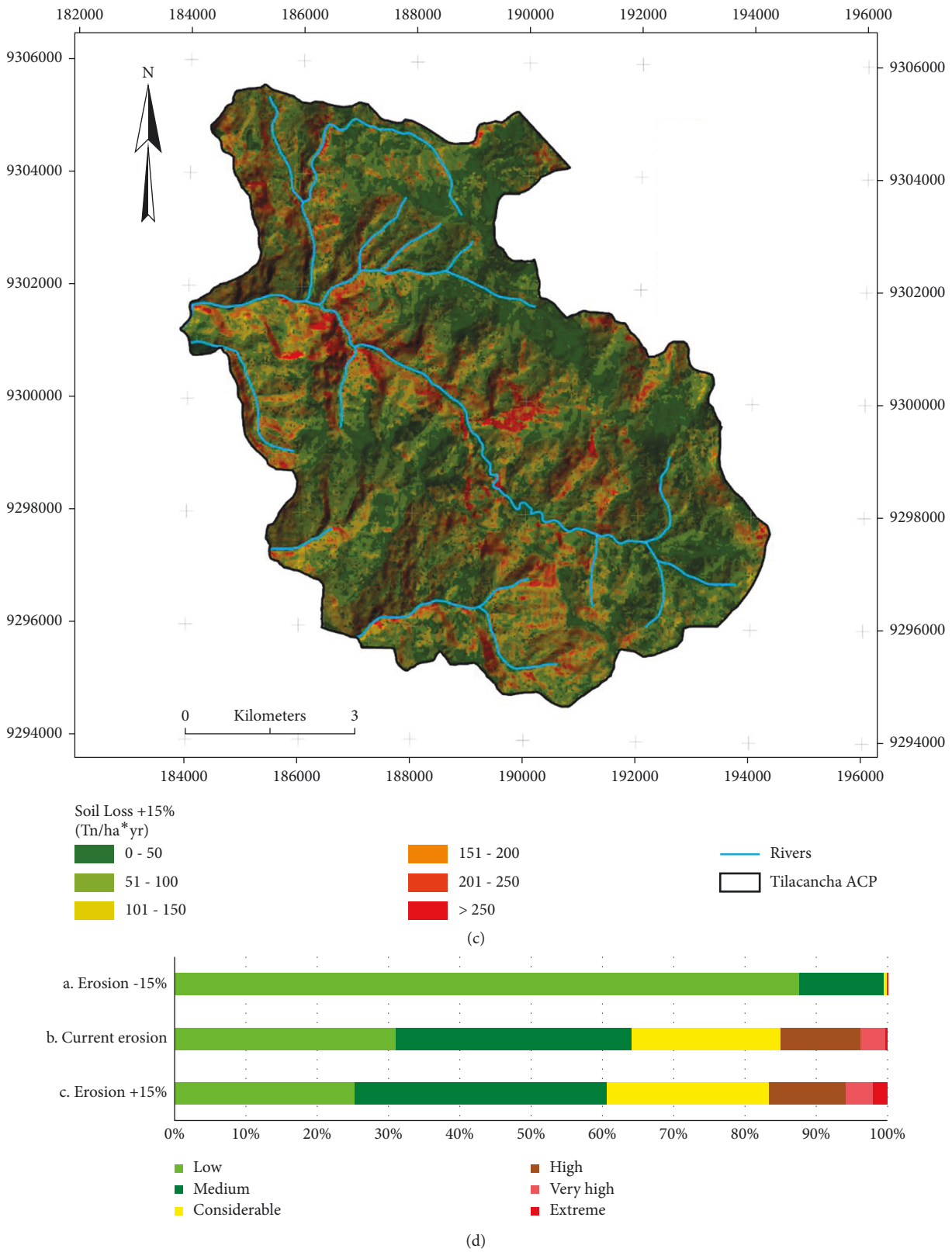

Figure 8: Precipitation maps for erosivity factor: (a) observed annual precipitation, (b) precipitation with a 15% decrease in the coefficient of variation of the historical data group, and (c) precipitation with a 15% increase in the coefficient of variation of the historical data group for the ACP.

Table 2: Comparison of soil loss for the year 2019 and two scenarios with a reduction of and an increase of 15% in annual rainfall for the ACP.

Soil loss (t/ha·yr)								
Level	Color	Value range	Observed rainfall (ha)	% area	(−) 15% rainfall (ha)	% area	(+) 15% rainfall (ha)	% area
Low		0.20–50	2113	31.1	5956	87.58	1722	25.3
Medium		51–100	2251	33.1	806	11.85	2397	35.2
Considerable		101–150	1414	20.8	34.9	0.51	1554	22.9
High		151–200	767	11.3	2.99	0.04	729.1	10.7
Very high		201–250	238.3	3.5	0.69	0.01	259.9	3.82
Extreme		>251	17.57	0.26	0.08	0.001	138.8	2.04
Total			6800	100	6800	100	6800	100

of 10 m determined greater precision more than the Landsat-7 ETM and the annual average of soil loss has been widely used to determine the causes of water erosion [62]. The average volume of soil eroded in Tilacancha was 60 t/ha.yr for the year 2019 in the ACP. The value exceeds averages for places that are also important for conserving water, such as the subhumid Gumara Basin where 42.67 t/ha.yr of lost soil volume was estimated [63], Anjeni Watershed, with 24.6 t/ha.yr [64], 47 93 t/ha.yr in Koga Watershed [56], Upper Blue Nile Basin 27.5 t/ha.yr [65], and Andassa Watershed 23.7 t/ha.yr [66]. The 69.59% of the Tilacancha ACP corresponded to erosion of 10 to 25 t/ha.yr, a value that doubles in range when compared with 74% of the total area of a Microbasin of the Madín Water Dam in Mexico where it erodes from 0–10 t/ha.yr [62].

Climate and land use trends contribute to reducing the volume of water infiltration and increasing the runoff generation [67]. Although the basic elements of water collection, storage, and discharge are not well understood in the ACP, subsurface runoff dominates the hydrology of the site and many humid and steep regions, predisposing surfaces to a greater volume of soil erosion [68]. For this reason, the precipitation scenarios were estimated in the ACP, a place that is subject to future increases in the intensity of precipitation, and are an important aspect of climate change [69]; warming will tend to accelerate the cycle general hydrological, intensifying wet extremes [70], in addition to dry extremes in some areas [69].

Likewise, variations in dry days and the intensity of precipitation in wet days account for more than half of the change in total annual precipitation in regions such as Peru (areas between 40°N and 40°S) [69] and consequently in Tilacancha. While it is an area that stores and provides water to the city of Chachapoyas, it is expected that its final destination will be focused on conservation, increasing the number of intense rains that allow greater capture and retention of the same. However, the values presented in the research suggest a relationship with the flows impacted by rain. They dominate the erosion of the sheet and between furrow and are important to erode the soil rich in nutrients and other chemical substances that can have harmful effects on water quality [71]. In the current models used to analyze climate, there is no consensus on how different parts of the earth will warm up; although global changes in extremes of temperature and precipitation since the mid-20th century are well studied, knowledge about the changes at century-scale is limited [72], and this uncertainty is understandable in the ACP after observing that the estimates of increase and reduction of 15% in rainfall lead to soil losses due to water erosion that would reach maximum volumes of 1028.84 t/ha.yr and 301.56 t/ha.yr, respectively.

The values confirm that water erosion is considered the most dangerous form of soil degradation [73]. Then, the monitoring of water erosion and the factors that control the loss of soil and water are essential for conservation planning [74].

5. Conclusions

USLE allowed estimating the loss of soil in the Tilacancha ACP. The factors were obtained individually based on the equations of the factors: rain erosivity (R) in 2019 and simulating increase and decrease of 15% of rainfall, soil erodibility (K), length and degree of slope (LS), coverage (C), and conservation practices (P). In 2019, there was a range of 0.4 to 665.2 t/ha.yr of soil lost by water erosion according to six ranges, ranging from low to extreme soil loss according to the spatial distribution of the volume of soil lost.

The estimates of the volume of soil lost due to water erosion under scenarios of decrease and increase in rainfall (±15%) demonstrated the need to act on urgent measures to mitigate erosion levels in the Tilacancha ACP, an important area that harbors water for the city of Chachapoyas, since, if there is a 15% reduction in precipitation, the ranges are estimated from 0.20 to 301.56 t/ha.yr of soil lost due to water erosion. However, if there is an increase of 15% of precipitation in the ACP, the ranges can go from 0.20 to 1028.84 t/ha.yr of soil lost by water erosion. Evaluation of proposals according to the level of loss and influence of each factor on the spatial distribution of erosion can be the beginning of a series of conservation strategies under climate change scenarios for the Tilacancha ACP.

Data Availability

Data are openly available: García, Ligia; Veneros, Jaris; Pereyra, César; Chávez, Segundo; Bustamante, Danilo;

Calderon, Martha S; Idrogo, Guillermo; and Morales, Eli (2020). Geospatial analysis of soil erosion including precipitation scenarios in a conservation area of the Amazon region in Peru: Figshare Dataset https://doi.org/10.6084/m9.figshare.13138331.v7.

Additional Points

Software: (1) ArcGis 10.7 was used to do map algebra for the USLE equation under the three scenarios. (2) QGIS 3.14 was used for the atmospheric correction of satellite images using the Semiautomatic Classification Plugin (SCP). Geolocation information: Amd0: Peru, Adm1: Amazonas, Adm2: Chachapoyas, and Adm3: Maino and Maino. Datum Projected Coordinate System: WGS_1984_UTM_Zone_18S.

Conflicts of Interest

The authors declare no conflicts of interest.

Authors' Contributions

J.V.; L.G.; S.C.; D.B; and M.C. conceptualized the study; L.G. and E.M. formulated the methodology; E.M. performed validation; J.V. and FPC. were responsible for the software; J.V.; L.G.; and S.C. conducted formal analysis; J.V. obtained resources; J.V. curated data; J.V.; L.G.; and S.C. prepared the original draft of the manuscript; L.G. reviewed and edited the manuscript; J.V. and FP. performed visualization; S.C. supervised the work; and J.V. acquired funding. All authors have read and agreed to the published version of the manuscript.

Acknowledgments

The authors would like to thank the members of the DRON-UNTRM Project, who accompanied them on the field trips to take samples for laboratory analysis and validate maps through 1500 georeferenced points. The authors also thank all the residents of the rural communities of Maino and Levanto for their support as guides in the ACP and for their important information provided. Finally, the authors thank all the people who supported us at the Toribio Rodríguez de Mendoza National University in Amazonas and the Municipal Drinking Water Company for all the logistics provided. This research was supported by the World Bank through the National Fund for Scientific, Technological Development, and Technological Innovation, FONDECYT by its acronym in Spanish, CONTRACT No. 161-2018-FONDECYT- BM- IADT- SE (Drone Project), and the CEINCAFE Public Investment Project (SNIP No. 352439 and CUI No. 2314883).

References

[1] N. Shanee, S. Shanee, and R. H. Horwich, "Effectiveness of locally run conservation initiatives in north-east Peru," *ORYX*, vol. 49, no. 2, pp. 239–247, 2015.

[2] SERNANP (Servicio Nacional de Áreas Naturales Protegidas por el Estado), *Áreas naturales protegidas de administración nacional con categoría definitiva*Lima, Peru, 2020, https://www.sernanp.gob.pe/documents/10181/165150/Listado+ANP+03.03.2020.pdf/47f02d7d-ee04-4e82-8c64-1d41668c92ff.

[3] R. Salas, E. Barboza, N. Rojas, and N. Rodriguez, "Deforestación en el área de conservación privada Tilacancha: zona de recarga hídrica y de abastecimiento de agua para Chachapoyas," *Rev. investig. agroproducción sustentable*, vol. 2, no. 3, pp. 54–64, 2018.

[4] MINAM (Ministerio del Ambiente de Perú), *Mapa Nacional de Ecosistemas*MINAM, San Martín, Peru, 2018, https://sinia.minam.gob.pe/mapas/mapa-nacional-ecosistemas-peru.

[5] W. Guzmán Castillo, E. S. Arellanos Carrión, and S. G. Chavez Quintana, "Determinación e incidencia de la disposición a pagar en esquemas de pagos por servicios ambientales hídricos: estudio de caso en las capitales de las provincias de Chachapoyas, Rodríguez de Mendoza y Utcubamba," *Folia Amazonica*, vol. 1, no. 2, pp. 141–151, 2012, https://pdfs.semanticscholar.org/da3f/1818ec19577be6eec3f31e8ffedfea5.pdf?_ga=2.196015148.1032884175.1597095336-821619953.1592514146.

[6] M. Vigo, L. Juárez, and M. Oliva, "Cosecha de agua de lluvia como tecnología de conservación de los manantiales amenazados, Chachapoyas," *Revista de Investigación de Agroproducción Sustentable*, vol. 3, no. 1, pp. 13–19, 2019.

[7] I. Soligno, A. Malik, and M. Lenzen, "Socioeconomic drivers of global Blue water use," *Water Resources Research*, vol. 55, no. 7, pp. 5650–5664, 2019.

[8] Y. Wada and M. F. P. Bierkens, "Sustainability of global water use: past reconstruction and future projections," *Environmental Research Letters*, vol. 9, no. 10, 2014.

[9] M.-P. Faucon, "Plant-soil interactions as drivers of the structure and functions of plant communities," *Diversity*, vol. 12, no. 12, p. 452, 2020.

[10] R. Morgan, "Estimating regional variations in soil erosion hazard in Peninsular Malaysia," *Malayan Nature Journal*, vol. 28, pp. 94–106, 1974, https://pascal-francis.inist.fr/vibad/index.php?action=getRecordDetail&idt=PASCALGEODEBRGM7620029622.

[11] B. Zhu, Z. Li, P. Li, G. Liu, and S. Xue, "Soil erodibility, microbial biomass, and physical-chemical property changes during long-term natural vegetation restoration: a case study in the Loess Plateau, China," *Ecological Research*, vol. 25, no. 3, pp. 531–541, 2010.

[12] H. K. Addis and A. Klik, "Predicting the spatial distribution of soil erodibility factor using USLE nomograph in an agricultural watershed, Ethiopia," *International Soil and Water Conservation Research*, vol. 3, no. 4, pp. 282–290, 2015.

[13] F. Gaspari, M. Delgado, and G. Denegri, "Estimación espacial, temporal y económica de la pérdida de suelo por erosión hídrica superficial," *Terra Latinoamericana*, vol. 27, no. 1, pp. 43–51, 2009, http://www.scielo.org.mx/pdf/tl/v27n1/v27n1a6.pdf.

[14] H. M. Rizeei, M. A. Saharkhiz, B. Pradhan, and N. Ahmad, "Soil erosion prediction based on land cover dynamics at the Semenyih watershed in Malaysia using LTM and USLE models," *Geocarto International*, vol. 31, no. 10, pp. 1158–1177, 2016.

[15] K. de Mello, "Forest cover and water quality in tropical agricultural watershed," Doctoral thesis, Escola Superior de Agricultura Luiz de Queiroz, Piracicaba, Brazil, 2017.

[16] N. Germany, P. Rendon, B. Steinhoff-Knopp, P. Saggau, and B. Burkhard, "Assessment of the relationships between agroecosystem 2 condition and soil erosion regulating

ecosystem service in Assessment of the relationships between agroecosystem," *bioRxiv*, 2020.

[17] Z. Tan, L. R. Leung, H. Y. Li, and T. Tesfa, "Modeling sediment yield in land surface and Earth system models: model comparison, development, and evaluation," *Journal of Advances in Modeling Earth Systems*, vol. 10, no. 9, pp. 2192–2213, 2018.

[18] MINAM (Ministerio del Ambiente de Perú), *Resolución Ministerial N° 118-2010-MINAM*, MINAM, Lima, Peru, 2010.

[19] W. Wischmeier and D. Smith, *Predicting Rainfall-Erosion Losses from Cropland East of the Rocky Mountains: Guide for Selection of Practices for Soil and Water Conservation*, United States Department of Agriculture, Washington, DC, USA, 282nd edition, 1965.

[20] H. Blanco-Canqui and R. Lal, *Principles of Soil Conservation and Management*, Springer, Amsterdam, Netherlands, 2010.

[21] C. Alewell, P. Borrelli, K. Meusburger, and P. Panagos, "Using the USLE: chances, challenges and limitations of soil erosion modelling," *International Soil and Water Conservation Research*, vol. 7, no. 3, pp. 203–225, 2019.

[22] C. J. L. M. Falcão, S. M. A. Duarte, and A. da Silva Veloso, "Estimating potential soil sheet Erosion in a Brazilian semi-arid county using USLE, GIS, and remote sensing data," *Environmental Monitoring and Assessment*, vol. 192, no. 1, 2020.

[23] B. H. Phan, N. Quoc Viet, P. A. Hung, L. X. Thai, L. S. Chinh, and N. X. Hai, "Integrated geographical information system (GIS) and remote sensing for soil erosion assessment by using universal soil loss equation (USLE): case study in Son La province," *VNU Journal of Science: Earth and Environmental Sciences*, vol. 35, no. 1, 2019.

[24] A. Demirci and A. Karaburun, "Estimation of soil erosion using RUSLE in a GIS framework: a case study in the Buyukcekmece Lake watershed, northwest Turkey," *Environmental Earth Sciences*, vol. 66, no. 3, pp. 903–913, 2012.

[25] W. . Wischmeier and D. . Smith, *Predicting Rainfall Erosion Losses:a Guide to Conservation Planning*, Department of Agriculture, Science and Education Administration, Washington, DC, USA, 1978.

[26] S. E. Fick and R. J. Hijmans, "WorldClim 2: new 1-km spatial resolution climate surfaces for global land areas," *International Journal of Climatology*, vol. 37, no. 12, pp. 4302–4315, 2017.

[27] C. Ballabio, P. Borrelli, J. Spinoni et al., "Mapping monthly rainfall erosivity in Europe," *The Science of the Total Environment*, vol. 579, pp. 1298–1315, 2017.

[28] D. Hernando and M. Romana, "Estimate of the (R)USLE rainfall erosivity factor from monthly precipitation data in mainland Spain," *Journal of Iberian Geology*, vol. 42, no. 1, pp. 113–124, 2016.

[29] S. Yin, M. A. Nearing, P. Borrelli, and X. Xue, "Rainfall Erosivity: an overview of methodologies and applications," *Vadose Zone Journal*, vol. 16, no. 12, 2017.

[30] L. A. Santos Acuña and C. A. González, "Mapa de Indices de Erodabilidad en la Cuenca Alta del Río Bogotá Utilizando el Sistema de Información Geográfica ARC-INFO," *Revistas Ingeniería e Investigación.*vol. 43, pp. 30–33, 1999.

[31] M. N. Cabrejos Valdivia, *Modelamiento geoespacial en la determinación del riesgo, vulnerabilidad y de la cuantificación de la erosión hídrica en la Microcuenca del Rio Atuen – Amazonas*, Universidad Nacional Agraria La Molina, Lima, Peru, 2016.

[32] J. M. Hernández Sánchez de los Dolores, D. S. Fernández Reynoso, M. R. Martínez Menez, B. F. Sandoval, E. R. Granados, and J. L. García Rodríguez, "Evaluation of slope stability in gullies from Huasca de Ocampo, Hidalgo, Mexico," *Terra Latinoam.*vol. 37, no. 3, pp. 303–313, 2019.

[33] Monroy-Rodríguez, F. Álvarez-Herrera, J. Alvarado-Sanabria, F. Liliana Monroy-Rodríguez, J. Giovanni Álvarez-Herrera, and H. Alvarado-Sanabria, "Spatial distribution of some fisical soil properties in a transect of the Tunguavita farm, Paipa," *Rev. U.D.C.A Actual. Divulg. Científica*, vol. 20, no. 1, pp. 91–100, 2017, https://revistas.udca.edu.co/index.php/ruadc/article/view/66/36.

[34] E. M. Romero-Lázaro, D. Ramos-Pérez, F. M. Romero, and S. Sedov, "Indirect indicators of residual contamination in soils and sediments of the Sonora river basin, Mexico," *Revista Internacional de Contaminación Ambiental*, vol. 35, no. 2, pp. 371–386, 2019.

[35] A. Walkley and I. A. Black, "An examination of Degtjareff method for determining soil organic matter and a proposed modification of the chromic acid titration method," *Soil Science*, vol. 37, no. 1, pp. 29–38, 1934, https://ui.adsabs.harvard.edu/abs/1934SoilS3729W/abstract.

[36] I. D. Moore and G. J. Burch, "Physical basis of the length-slope factor in the universal soil loss equation 1," *Soil Science Society of America Journal*, vol. 50, no. 5, pp. 1294–1298, 1986.

[37] I. D. Moore and G. J. Burch, "Modelling erosion and deposition: topographic effects," *Transactions of the ASAE*, vol. 26, pp. 1624–1630, 1986.

[38] A. G. Barrios and E. Quiñonez, "Evaluación de la erosión utilizando el modelo (R) USLE, con apoyo de SIG: aplicación en una microcuenca de Los Andes venezolanos," *Revista Forestal Venezolana*, vol. 4, no. 1, pp. 65–71, 2000, http://www.saber.ula.ve/handle/123456789/24173.

[39] A. F. Castro Quintero, L. A. Lince Salazar, and O. Riaño Melo, "Determinación del riesgo a la erosión potencial hídrica en la zona cafetera del Quindío, Colombia," *Revista de Investigacion Agraria y Ambiental*, vol. 8, no. 1, pp. 2145–6097, 2017, https://hemeroteca.unad.edu.co/index.php/riaa/article/view/1828.

[40] K. Hogenson, S. A. Arko, B. Buechler, R. Hogenson, J. Herrmann, and A. Geiger, "Hybrid Pluggable Processing Pipeline (HyP3): a cloud-based infrastructure for generic processing of SAR data," in *AGUFM*vol. 2016, 2016, https://ui.adsabs.harvard.edu/abs/2016AGUFMIN21B1740H/abstract.

[41] J. Ngula Niipele and J. Chen, "The usefulness of alos-palsar dem data for drainage extraction in semi-arid environments in the Iishana sub-basin," *Journal of Hydrology: Regional Studies*, vol. 21, pp. 57–67, 2019.

[42] S. Nitheshnirmal, P. Thilagaraj, S. A. Rahaman, and R. Jegankumar, "Erosion risk assessment through morphometric indices for prioritisation of Arjuna watershed using ALOS-PALSAR DEM," *Modeling Earth Systems and Environment*, vol. 5, no. 3, pp. 907–924, 2019.

[43] H. E. Flores López, M. Martínez Menes, J. L. Oropeza Mota, E. Mejía Saens, and R. Carrillo González, "Integration of the USLE to a GIS to estimate the soil erosion by water in a watershed of Tepatitlán, Jalisco, Mexico," *Terra*, vol. 21, no. 2, pp. 233–244, 2003, https://www.redalyc.org/pdf/573/57315595010.pdf.

[44] P. Desmet and G. Govers, "A GIS procedure for automatically calculating the USLE LS factor on topographically complex landscape units," *Journal of Soil and Water Conservation*, vol. 51, no. 5, pp. 427–434, 1996, https://go.gale.com/ps/i.do?p=AONE&sw=w&issn=00224561&v=2.1&it=r&id=GALE%7CA18832564&sid=googleScholar&linkaccess=fulltext.

[45] Z. H. Shi, C. F. Cai, S. W. Ding, T. W. Wang, and T. L. Chow, "Soil conservation planning at the small watershed level using RUSLE with GIS: a case study in the Three Gorge Area of China," *Catena*, vol. 55, no. 1, pp. 33–48, 2004.

[46] M. Hasmadi, P. Hz, and S. Mf, "Evaluating supervised and unsupervised techniques for land cover mapping using remote sensing data," *Malaysian Journal of Society and Space*, vol. 5, no. 1, pp. 1–10, 2009, http://journalarticle.ukm.my/917/1/1.2009-1-hasmadi-english.pdf.

[47] W. Gong, Z. Zhu, P. Li et al., "Mobile aerosol lidar for Earth observation atmospheric correction," in *Proceedings of the 2006 IEEE International Symposium on Geoscience and Remote Sensing*, Denver, CO, USA, July-August 2006.

[48] T. D. Acharya and I. Yang, "Exploring Landsat 8," *International Journal of Engineering and Applied Sciences*, vol. 4, no. 4, pp. 2319–4413, 2015, http://earthobservatory.nasa.gov/IOTD/.

[49] M. J. Arango Gutiérrez, W. Branch Bedoya, and V. B. Fernández, "Clasificación no supervisada de coberturas vegetales sobre imágenes digitales de sensores remotos: Landsat – Etm+," *Revista Facultad Nacional de Agronomía Medellín*, vol. 58, no. 1, pp. 2611–2634, 2005, http://www.scielo.org.co/pdf/rfnam/v58n1/a04v58n1.pdf.

[50] R. Vagaría Alfonso and G. Fernanda, "Estimación de la admisibilidad de pérdidas de suelo por erosión hídrica en la cuenca del arroyo Napaleofú, provincia de Buenos Aires-Argentina," *Revista Geografica Venezolana*, vol. 56, no. 1, pp. 105–119, 2013, http://www.saber.ula.ve/bitstream/handle/123456789/40100/articulo6.pdf?sequence=1&isAllowed=y.

[51] H. A. Pacheco, R. X. Cevallos, and C. J. Vinces, "Cálculo del factor C de la RUSLE, en la cuenca del río Carache, Trujillo-Venezuela usando imágenes del Satélite Miranda VRSS-1 Calculation of RUSLE C factor in Carache river basin, Trujillo, Venezuela Satellite Images using Miranda VRSS-1," *Revista Espacios*, vol. 40, no. 3, p. 6, 2019, http://www.revistaespacios.com/a19v40n03/a19v40n03p06.pdf.

[52] J. V. Prado-Hernández, P. Rivera-Ruiz, B. De León-Mojarro, M. Carrillo-García, A. Martínez-Ruiz, and A. Responsable, "Calibración de los modelos de pérdidas de suelo usle y musle en una cuenca forestal de México: caso el Malacate," *Agrociencia*, vol. 51, pp. 265–284, 2017, http://www.scielo.org.mx/pdf/agro/v51n3/1405-3195-agro-51-03-00265-en.pdf.

[53] D. Rozos, H. D. Skilodimou, C. Loupasakis, and G. D. Bathrellos, "Application of the revised universal soil loss equation model on landslide prevention. An example from N. Euboea (Evia) Island, Greece," *Environmental Earth Sciences*, vol. 70, no. 7, pp. 3255–3266, 2013.

[54] W. Buytaert, R. Célleri, B. De Bièvre, and F. Cisneros, "Hidrología del páramo andino: propiedades, importancia y vulnerabilidad," *Revista Facultad Nacional de Agronomía Medellín*, vol. 2, pp. 8–27, 2012, http://paramo.cc.ic.ac.uk/pubs/ES/Hidroparamo2.pdf.

[55] G. R. Foster and W. H. Wischmeier, "Evaluating irregular slopes for soil loss prediction," *Transactions of the American Society of Agricultural Engineers*, vol. 17, no. 2, pp. 0305–0309, 1974.

[56] H. S. Gelagay and A. S. Minale, "Soil loss estimation using GIS and Remote sensing techniques: a case of Koga watershed, Northwestern Ethiopia," *International Soil and Water Conservation Research*, vol. 4, no. 2, pp. 126–136, 2016.

[57] W. Wischmeier, D. Wight, and D. Smith, "Rainfall energy and its relationship to soil loss," *American Geophysical Union*, vol. 39, no. 2, p. 258, 1958, https://agupubs.onlinelibrary.wiley.com/doi/10.1029/TR039i002p00285.

[58] C. Ballabio, P. Borrelli, J. Spinoni et al., "Mapping monthly rainfall erosivity in Europe," *The Science of the Total Environment*, vol. 579, pp. 1298–1315, 2017.

[59] D. Escobar, *Estimación de la erosión hídrica en zona semiárida del norte chileno mediante la ecuación universal de pérdida de suelo (USLE): el caso de Ounitaqui (Iv Región de Coquimbo)*, Universidad de Chile, Santiago, Chile, 2019.

[60] J. A. Thompson, J. C. Bell, and C. A. Butler, "Digital elevation model resolution: effects on terrain attribute calculation and quantitative soil-landscape modeling," *Geoderma*, vol. 100, pp. 67–89, 2001, http://www.elsevier.nlrlocatergeoderma.

[61] T. M. Basuki, A. K. Skidmore, Y. A. Hussin, and I. van Duren, "Estimating tropical forest biomass more accurately by integrating ALOS PALSAR and Landsat-7 ETM+ data," *International Journal of Remote Sensing*, vol. 34, no. 13, pp. 4871–4888, 2013.

[62] I. Castro Mendoza, "Estimación de pérdida de suelo por erosión hídrica en microcuenca de presa Madín, México," *Ingenieria Hidraulica y Ambiental*, vol. 34, no. 2, pp. 3–16, 2013, http://scielo.sld.cu/pdf/riha/v34n2/riha01213.pdf.

[63] M. Belayneh, T. Yirgu, and D. Tsegaye, "Potential soil erosion estimation and area prioritization for better conservation planning in Gumara watershed using RUSLE and GIS techniques," *Environmental Systems Research*, vol. 8, no. 1, 2019.

[64] S. G. Setegn, B. Dargahi, R. Srinivasan, and A. M. Melesse, "Modeling of sediment yield from anjeni-gauged watershed, Ethiopia using SWAT model," *Journal of the American Water Resources Association*, vol. 46, no. 3, pp. 514–526, 2010.

[65] N. Haregeweyn, A. Tsunekawa, J. Poesen, and M. Tsubo, "Comprehensive assessment of soil erosion risk for better land use planning in river basins: case study of the Upper Blue Nile River," *The Science of the Total Environment*, vol. 574, pp. 95–108, 2017.

[66] T. Gashaw, T. Tulu, M. Argaw, and A. W. Worqlul, "Evaluation and prediction of land use/land cover changes in the Andassa watershed, Blue Nile Basin, Ethiopia," *Environmental Systems Research*, vol. 6, no. 1, 2017.

[67] S. Beganskas, K. S. Young, A. T. Fisher, R. Harmon, and S. Lozano, "Runoff modeling of a coastal basin to assess variations in response to shifting climate and land use: implications for managed recharge," *Water Resources Management*, vol. 33, no. 5, pp. 1683–1698, 2019.

[68] T. Sayama, J. J. Mcdonnell, A. Dhakal, and K. Sullivan, "How much water can a watershed store?" *Hydrological Processes*, vol. 25, no. 25, pp. 3899–3908, 2011.

[69] S. D. Polade, D. W. Pierce, D. R. Cayan, A. Gershunov, and M. D. Dettinger, "The key role of dry days in changing regional climate and precipitation regimes," *Scientific Reports*, vol. 4, 2014.

[70] P. Y. Groisman, R. W. Knight, D. R. Easterling, T. R. Karl, G. C. Hegerl, and V. N. Razuvaev, "Trends in intense precipitation in the climate record," *Journal of Climate*, vol. 18, pp. 1326–1350, 2005.

[71] P. I. Kinnell, "Simulations demonstrating interaction between coarse and fine sediment loads in rain-impacted flow," *Earth Surface Processes and Landforms*, vol. 31, no. 3, pp. 355–367, 2006.

[72] M. G. Donat, L. V. Alexander, N. Herold, and A. J. Dittus, "Temperature and precipitation extremes in century-long gridded observations, reanalyses, and atmospheric model simulations," *Journal of Geophysical Research*, vol. 121, no. 19, pp. 11174–11189, 2016.

[73] T. K. Alexandridis, A. M. Sotiropoulou, G. Bilas, N. Karapetsas, and N. G. Silleos, "The Effects of seasonality in

estimating the C-Factor of soil erosion studies," *Land Degradation & Development*, vol. 26, no. 6, pp. 596–603, 2015.

[74] B. P. Silva Christofaro, M. L. Silva Naves, P. V. Batista Gomes, L. Pontes Machado, E. F. Araújo, and N. Curi, "Perdas de solo e água em plantios de eucalipto e floresta nativa e determinação dos fatores da USLE em sub-bacia hidrográfica piloto no Rio Grande do Sul, Brasil," *Ciencia E Agrotecnologia*, vol. 40, no. 4, pp. 432–442, 2016.